Journal of Energy Storage 55 (2022) 105509

Contents lists available at ScienceDirect

Journal of Energy Storage

journal homepage: www.elsevier.com/locate/est

Research Paper

A hybrid energy storage system based on self-adaptive variational mode decomposition to smooth photovoltaic power fluctuation

Gang Xiao [a], Fen Xu [a], Lianghuai Tong [b], Haoran Xu [a], Peiwang Zhu [a,*]

[a] State Key Laboratory of Clean Energy Utilization, Zhejiang University, 38 Zheda Road, Hangzhou 310027, China
[b] Quzhou Special Equipment Inspection Center, 592 Leyuan Road, Quzhou 324000, China

ARTICLE INFO

Keywords:
Smooth photovoltaic (PV) power fluctuation
Hybrid energy storage system (HESS)
Variational mode decomposition (VMD)
Hilbert transform
Economic evaluation

ABSTRACT

The fluctuation and randomness of photovoltaic (PV) power generation can adversely affect the stable operation of the grid. The use of a hybrid energy storage system (HESS) can reduce the impact on the grid caused by PV power fluctuation. To improve the reliability and economy of the HESS, it is important to choose a reasonable power signal analysis method in the smoothing process. In this regard, a HESS based on self-adaptive variational mode decomposition (VMD) is proposed in this paper to smooth PV power fluctuation. This method determines the number of decomposed modes and grid-connected modes adaptively. Moreover, the VMD-Hilbert method is used to allocate the power of HESS to lead-carbon batteries and supercapacitors. In addition, a HESS economic evaluation model is developed. The results indicate that after self-adaptive VMD, the PV power fluctuation rate in different weather conditions is reduced to 9.68 %/5 min, 9.49 %/5 min, and 8.19 %/5 min respectively, which is lower than that before smoothing and meets the PV grid-connected fluctuation standard. Due to the optimization of grid-connected mode number, the power of HESS can reduce by 17.36 % on sunny days. Also, the HESS life cycle annualized cost in the maximum fluctuation weather condition reduces by 24.89 % compared to when empirical mode decomposition (EMD) is used.

1. Introduction

As the world faces a crisis of energy depletion, the development of new energy is imminent. Thus, the new clean energy represented by photovoltaic (PV) is gradually being developed [1,2]. However, due to the characteristics of uncertainty, randomness and fluctuation, PV power generation seriously affects the normal operation of the grid in large-scale PV grid connections and brings severe challenges to the

Nomenclature: PV, photovoltaic; HESS, hybrid energy storage system; VMD, variational mode decomposition; EMD, empirical mode decomposition; SOC, state of charge; EEMD, ensemble empirical mode decomposition; P_{PV}, original PV power; P_g, grid-connected PV power after being suppressed by HESS; P_{HESS}, power of HESS; P_b, power of lead-carbon batteries; P_c, power of supercapacitors; WT, wavelet transform; FFT, fast Fourier transform; STFT, short time Fourier transform; WVT, Wigner-Ville transform; BDC, bi-directional DC-DC converter; EMS, energy management system; PCS, power conversion system; BMS, battery management system; SMS, supercapacitor management system; X_i, meteorological feature vector; I_i, average irradiance; T_i, average temperature; H_i, average relative humidity; L_i, irradiation duration; IMF, intrinsic mode function; k, number of decomposition mode; ω_k, corresponding center frequency of the mode; r, residual of VMD; ∂_t, the partial derivative with time t; $\delta(t)$, Dirac distribution function; u_k, mode component of VMD; $f(t)$, original signal; α, penalty factor; $\lambda(t)$, Lagrange multiplier; ADMM, alternate direction method of multipliers; ε, given determination accuracy; k_1, number of grid-connected mode; R, fluctuation rate of PV power; P_{rated}, installed PV capacity; T_{ET}, equivalent time of energy storage component; E_s, rated capacity of the energy storage component; P_r, rated power of the energy storage component; T_T, response time of the energy storage component; ω_T, response frequency of the energy storage component; $\alpha_k(t)$, instantaneous amplitude; $\psi_k(t)$, instantaneous phase; $\omega_k(t)$, instantaneous frequency of each mode component; ω_f, dividing point of high-frequency and low-frequency; VHT, VMD-Hilbert method; E_k, instantaneous energy; E_{mixing}, mode mixing energy; C_{HESS}, life cycle cost annualized model of HESS; C_{cap}, initial investment cost of HESS; C_{rep}, replacement cost of HESS; C_{maint}, maintenance cost of HESS; C_{bp}, cost per unit power of lead-carbon batteries; C_{be}, cost per unit capacity of lead-carbon batteries; C_{cp}, cost per unit power of supercapacitors; C_{ce}, cost per unit capacity of supercapacitors; E_b, capacity of lead-carbon batteries; E_c, capacity of supercapacitors; γ, discount rate of capital; T_{rt}, life cycle of HESS; n_b, replacement times of lead-carbon batteries in the life cycle; n_c, replacement times of supercapacitors in the life cycle; C_{b_maint}, average annualized maintenance cost per unit capacity of lead-carbon batteries; C_{c_maint}, average annualized maintenance cost per unit capacity of supercapacitors; RMSE, root mean square error; MAPE, mean absolute percentage error; P_i, actual PV power; P_i*, predicted PV power; n, amount of data.

* Corresponding author.
E-mail address: zhupw@zju.edu.cn (P. Zhu).

https://doi.org/10.1016/j.est.2022.105509
Received 1 March 2022; Received in revised form 6 July 2022; Accepted 15 August 2022
Available online 6 September 2022

power quality and stability of the grid [3–5]. In this regard, the energy storage system can make a difference. The use of energy storage technology charging/discharging can flexibly adjust the characteristics of power imbalance and smooth the fluctuation of PV output power, which is an important means to effectively reduce the impact of PV power fluctuation on the grid and improve grid stability [6–8]. Energy storage can be divided into physical energy storage, chemical energy storage, thermal energy storage and electrical energy storage [9]. However, single energy storage has its limitations, because it is difficult to meet the characteristics of high energy density, high power density and long service life at the same time. A hybrid energy storage system (HESS) makes up for the deficiencies of characteristics of a single energy storage system to achieve complementary advantages. Therefore, the use of HESS to smooth PV power fluctuation attracts attention in recent years [10,11].

In this paper, HESS is composed of lead-carbon batteries and supercapacitors. Lead-carbon batteries are based on traditional lead-acid batteries with a capacitive improvement on the negative electrode material [12]. Lead-carbon batteries combine the advantages of both lead-acid batteries and supercapacitors. Carbon addition prevents sulfation of the negative electrode, significantly improving the service life of the battery [13,14]. Lead-carbon batteries have high safety, long cycle life and low cost. Lead-carbon battery is a kind of chemical battery for energy storage with potential commercial application and development prospects, which is suitable for large-scale and high safety occasions. Supercapacitors not only have the characteristics of rapid charge and discharge of traditional capacitors but also have the energy storage characteristics of batteries. At present, supercapacitors are widely used together with batteries [15].

After determining the composition of the HESS, the reasonable power allocation and operation control algorithm is the key to smooth the PV power fluctuation. However, some conventional algorithms are susceptible to power signal instability. This leads to insufficient PV power fluctuation smoothing to meet the volatility criterion, or excessive smoothing to make the storage device capacity larger and less economical. Scholars at home and abroad have conducted a lot of research on algorithms for smoothing PV power fluctuation with HESS, and have obtained relevant results. Wang et al. [16] proposed a low-pass filtering algorithm with threshold judgment to decide whether the energy storage system is working by judging the magnitude of fluctuation. Ding et al. [17] and Zhou et al. [18] used the self-adaptive wavelet packet decomposition technique to decompose the wind power into different frequency components and proposed the primary power allocation within HESS. But the wavelet packet decomposition must make a secondary correction to the power command, which makes the calculation process complex. Wu et al. [19] proposed to use the wavelet packet decomposition method to analyze the amplitude-frequency of PV grid-connected power. The charging and discharging power of each system are obtained according to the characteristics of different energy storage systems. At the same time, the fuzzy control method is used to adaptively control the state of charge (SOC) of the supercapacitor. However, the wavelet packet decomposition algorithm does not have the adaptive capability only by setting the threshold value to eliminate the real-time delay problem of wavelet packet decomposition. Tian et al. [20] and He et al. [21] proposed to use empirical mode decomposition (EMD) to achieve the active power distribution, but the noise in the EMD decomposition process is relatively large, which is prone to mode mixing. To solve the problem of mode mixing, Sanabria-Villamizar et al. [22] and Sánchez-Sutil et al. [23] proposed to use ensemble empirical mode decomposition (EEMD) technique to reduce the mode mixing phenomenon and the edge effect. Then the Hilbert spectrum was used to identify frequency variations in the time domain. Wang et al. [24] and Jia et al. [25] proposed EEMD to achieve the distribution of active power. The high-frequency and low-frequency power was obtained by a temporal and spatial filter. However, due to the instability and nonlinear characteristics of the PV power signal, the filtering order of the temporal and spatial filter cannot be accurately determined. Moreover, the EEMD is noisy, which makes the power signal extraction inaccurate. Currently, the commonly used low-pass filtering, wavelet packet decomposition, EMD, EEMD and other methods have problems such as delay, poor accuracy, and mode mixing. VMD can solve the above problems to a certain extent [26].

Table 1
Performance comparison of common energy storage batteries [31–33].

Energy storage batteries	Advantages	Disadvantages
Lithium iron phosphate battery	High efficiency, high power density, high energy density	Safety issues such as battery heating and burning due to overcharging
Vanadium liquid flow battery	Mature technology, long cycle life	Low power density and energy density
Lead-acid battery	Low price, high safety	Low energy density, short life span
Lead-carbon battery	Long cycle life, high safety	Not high energy density

VMD uses the alternating direction multiplier method, which has good local optimization in anti-noise and processing non-stationary abrupt signals and is more suitable for smoothing PV power fluctuation [27,28]. However, the conventional VMD algorithm has an obvious drawback. Before using the VMD algorithm for signal processing, the decomposition mode number needs to be set in advance, it directly affects the final decomposition results. If the preset number of decomposition modes is not reasonable, it may lead to insufficient decomposition or over-decomposition resulting in mode mixing. Therefore, the determination of decomposition mode number occupies a crucial position in the VMD algorithm. Zhang et al. [29] proposed to determine the decomposition mode number by observing whether the center frequency of each mode is overlapped after VMD, then select the decomposition mode number by merit. But this method has no clear measurement criteria and is highly subjective. Moreover, it cannot be determined automatically by the program directly. It also requires multiple decompositions of the analyzed signal, which is a large workload. The conventional VMD algorithm only utilizes the first mode component obtained from the decomposition, without considering the influence of the remaining components on the results [30]. This algorithm applied to smooth PV power fluctuation may result in low grid-connected power and high HESS power. Therefore, this paper proposes a self-adaptive VMD, which can determine the decomposition mode number adaptively. Also the remaining components except the first mode component are taken into account to reduce the HESS power.

In summary, this paper uses a HESS based on self-adaptive VMD algorithm to smooth PV power fluctuation. Firstly, the original power of typical PV output scenarios is subjected to self-adaptive VMD. According to the grid-connected PV power fluctuation standard, the original PV power is decomposed into grid-connected power and HESS power, to achieve the maximum grid-connected power under the premise of smoothing PV power fluctuation. Secondly, the VMD-Hilbert method is applied to the HESS power to determine the frequency division point by the marginal spectrum obtained from time integration. The high-frequency signal and the low-frequency signal are assigned to the supercapacitors and the lead-carbon batteries respectively. Then, a life cycle annualized cost model is established for the economic evaluation of HESS. Finally, combined with the actual output data of a PV power station, the correctness of the model in this paper is verified.

2. PV-HESS system based on self-adaptive VMD

HESS can timely store and release the output power of PV power station through charging and discharging, so it has become the main means to solve the fluctuation of grid-connected PV power. Therefore, reasonable energy storage components and control strategies for PV

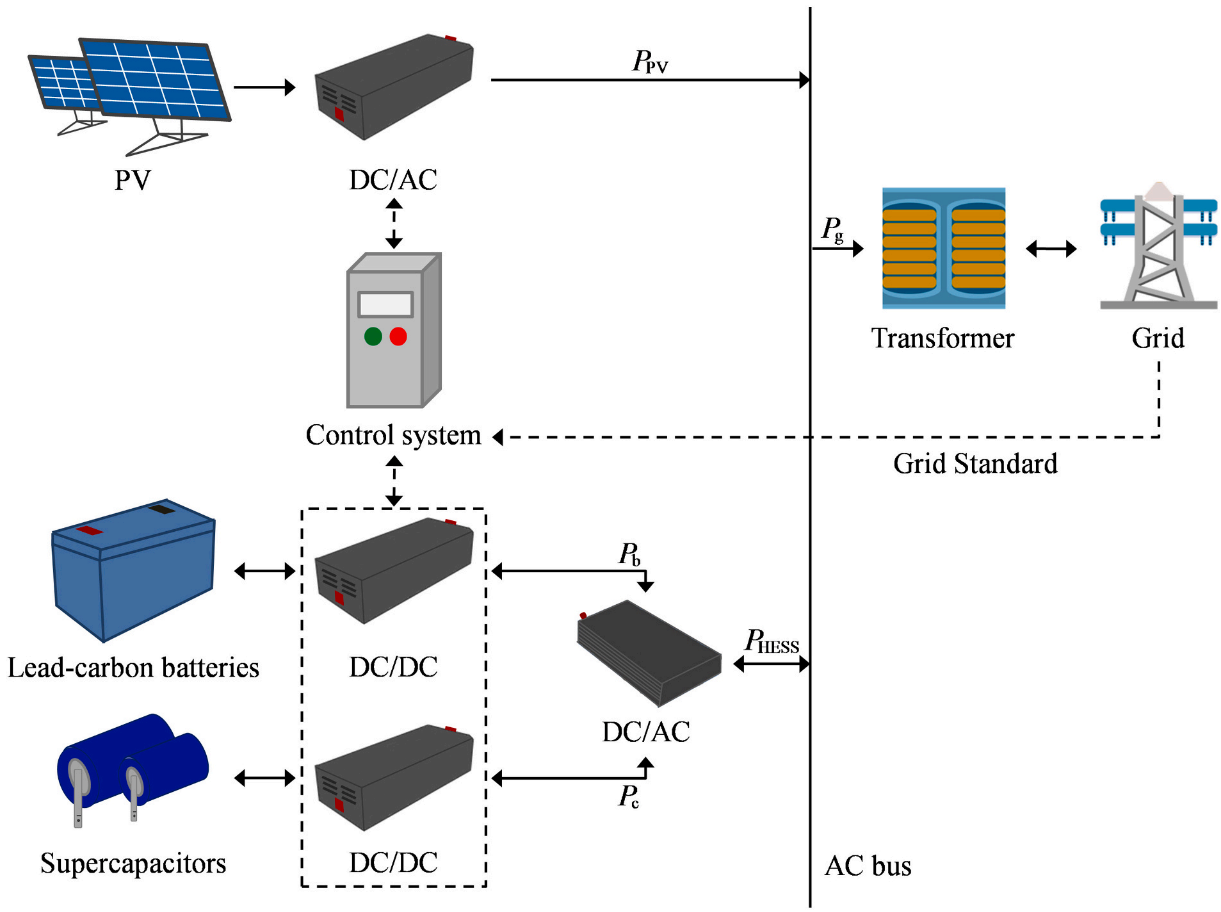

Fig. 1. Schematic diagram of grid-connected PV-HESS system.

power stations can reduce PV power fluctuation rate and improve power quality.

2.1. PV-HESS system structure and characteristic analysis

2.1.1. Selection of energy storage components

Energy storage batteries for HESS include lithium iron phosphate batteries, vanadium liquid flow batteries, lead-acid batteries and lead-carbon batteries, etc. A comparison of common battery performance is shown in Table 1. Therefore, the energy storage batteries in this paper are selected from lead-carbon batteries with long cycle life and high safety.

Table 2
Common algorithms for smoothing PV power fluctuation with HESS.

Algorithms	Performance analysis
Statistical analysis	Simple calculation, require high integrity and accuracy of historical statistical data
Fast Fourier transform (FFT)	Based on Fourier transform, fast calculation speed, there are aliasing and leakage in spectrum analysis
Short time Fourier transform (STFT)	Based on Fourier transform, the window width is fixed and cannot be adjusted adaptively
Wavelet transform (WT)	A signal time-frequency analysis method, the wavelet basis function lacks adaptability
Wigner-Ville transform (WVT)	Do not involve window function, interfered by cross term when analyzing multi-component signal
Low-pass filtering	Simple calculation, phase lag
Wavelet packet decomposition	Provide finer decomposition of high frequency signals, susceptible to the influence of fundamental waves
EMD	No need to set basis function, there is mode mixing phenomenon
EEMD	High noise, making the power signal extraction inaccurate
VMD	Good local optimization in noise immunity and handling of non-stationary burst signals

The HESS selected in this paper is composed of lead-carbon batteries and supercapacitors. Lead-carbon batteries have the advantages of high energy density and low cost, but their response speed is slow and the service life is greatly affected by the number of charging and discharging cycles, so they are used as energy type storage. Supercapacitors have fast response speed and long service life, however, they have relatively low energy density and high cost. They are suitable for the task of fast charging and discharging and frequent switching in the energy storage system, so they are used as power type storage. In this regard, lead-carbon batteries and supercapacitors can just complement each other in terms of technical performance. By forming a HESS with lead-carbon batteries and supercapacitors to give full play to the advantages of both types of energy storage, not only can the service life of the batteries be extended, but also the overall response and smoothing performance of HESS can be greatly improved.

2.1.2. PV-HESS system structure

The grid-connected structure of the PV-HESS system designed in this paper is shown in Fig. 1. The system consists of three main components: the PV power generation, HESS consisting of lead-carbon batteries and supercapacitors, and the control system. PV power generation is a clean energy generation method that converts solar energy into electricity through the photovoltaic effect. Due to the influence of various frequent meteorological factors such as rainfall and cloud movement, PV power generation has great fluctuation and will have an impact on the grid if directly connected to the grid. The role of the control system is to collect the real-time power signal of the PV power generation. Under the PV

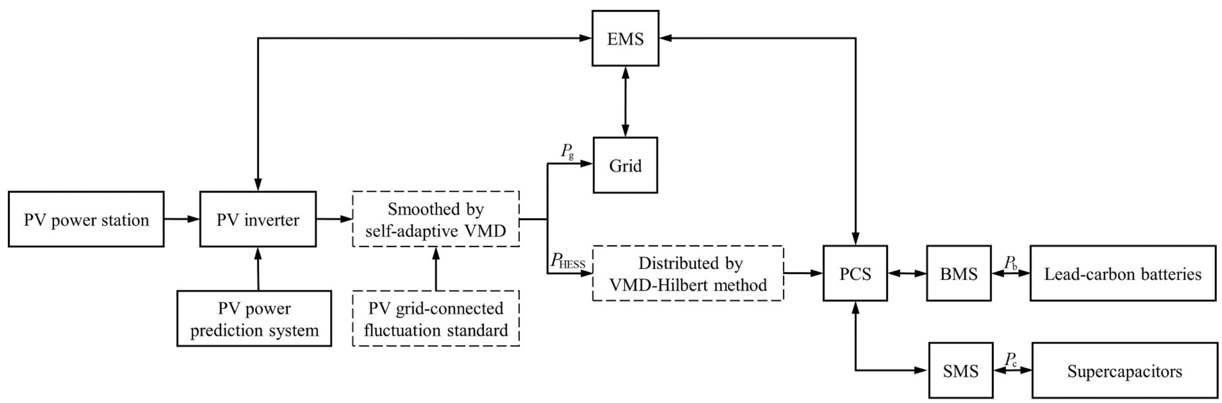

Fig. 2. Overall diagram of the PV-HESS system control process.

power fluctuation standard, control system adjusts the power of the HESS in real time, thereby smooth the fluctuation of PV output power and ensure the stable operation of the power grid.

In Fig. 1, P_{PV} is the original PV power, P_g is the grid-connected PV power after being suppressed by HESS, P_{HESS} is the power of HESS, P_b is the power of lead-carbon batteries, P_c is the power of supercapacitors. The HESS power consists of the power of lead-carbon batteries and the power of supercapacitors. By configuring the HESS, the power delivered from PV to the grid becomes the difference between the actual power from PV power generation and the HESS power, as shown in Eqs. (1) and (2):

$$P_{HESS} = P_b + P_c \tag{1}$$

$$P_g = P_{PV} - P_{HESS} \tag{2}$$

2.2. *Working principle of PV-HESS system*

2.2.1. *Comparative analysis between VMD and other algorithms*

Using a HESS to smooth PV power fluctuation, it is important to choose a suitable algorithm. Table 2 shows common algorithms for smoothing PV power fluctuation with HESS [34–39]. The traditional signal analysis is based on the Fourier transform. Because Fourier transform uses a global transform, for non-stationary signals, the Fourier transform expresses the local properties of time-frequency. Many new signal analysis algorithms have emerged based on Fourier transform. Wavelet transform (WT) is a time-frequency analysis method of signal, which can deal with non-stationary signals such as PV power well. In wavelet transform, the wavelet basis function needs to be selected first, which lacks adaptability. EMD is a new adaptive time-frequency analysis method. It is simple to operate and does not need to select a function similar to wavelet basis in advance, which overcomes the disadvantage of lack of adaptability of wavelet transform. However, EMD also has some disadvantages such as mode mixing and the edge effect. For different signals, each algorithm has its advantages and disadvantages. So the proper algorithm should be selected according to the characteristics of the signal. Since VMD has outstanding advantages in frequency extraction and mode separation with high noise robustness and mode aliasing suppression [28], VMD is chosen in this paper to smooth PV power fluctuation.

2.2.2. *PV-HESS system control strategy*

In order to improve the performance of HESS, the combination of lead-carbon batteries and supercapacitors can give full play to the advantages of both. In this paper, the lead-carbon batteries and supercapacitors are connected to the grid through a bi-directional DC/DC converter (BDC) and a DC/AC converter. The BDC is at the core of HESS [40]. The BDC has many functions, not only can it realize the energy storage and release at the same time, but also can improve the utilization rate of the battery to achieve stable output. Most importantly, the BDC can stabilize the DC bus voltage and reduce voltage fluctuation, thus improving the stability of the system. Therefore, the bi-directional Buck-Boost is chosen as the DC/DC converter topology in this paper. When the converter operates in the Buck circuit model, the energy flows from the bus to the energy storage system; when the converter operates in the Boost circuit model, the energy changes direction and flows from the energy storage system to the bus.

Fig. 2 shows an overall diagram of the PV-HESS system control process. Firstly, the PV power prediction system collects the real-time radiation value, temperature and other meteorological information of the PV power station, then predicts P_{PV} based on the historical and measured data of the PV power station [41]. Self-adaptive VMD is used to determine the grid-connected PV power and the HESS power. The high-frequency and low-frequency components are obtained by using the VMD-Hilbert method, thus the operation of each energy storage element is obtained. The PV inverter converts the direct current generated by PV generation into alternating current and achieves maximum output power through the Maximum Power Point Tracking method [42]. Energy management system (EMS) is the control core of the system, which summarizes the information of various components in the PV-HESS system and receives dispatching instructions from the grid. It not only controls the operation of the system comprehensively, but also makes decisions to ensure the safe operation of the system [43]. Power conversion system (PCS) is an executive device. PCS receives EMS commands through communication to control the charging and discharging process, to realize the regulation of active power and reactive power of the grid [44]. Battery management system (BMS) and supercapacitor management system (SMS) are responsible for the monitoring, evaluation and protection of lead-carbon batteries and supercapacitors respectively. Overcharging and over-discharging will shorten the life of lead-carbon batteries and supercapacitors. PCS can communicate with BMS and SMS for protective charge and discharge of lead-carbon batteries and supercapacitors, so as to ensure SOC changing in a reasonable range and meeting the power output requirement [45,46].

2.3. *PV power prediction model*

In order to achieve real-time control of HESS, PV power prediction is required. In this paper, a PV power prediction method based on similar days selection and Elman neural network model is used. Similar days are selected according to different weather conditions, and the Elman neural network is established to predict the PV power in three different weather conditions respectively.

2.3.1. *Selection of similar days*

PV power generation is affected by many meteorological factors, this paper selects the factors that have a greater impact on power, such as

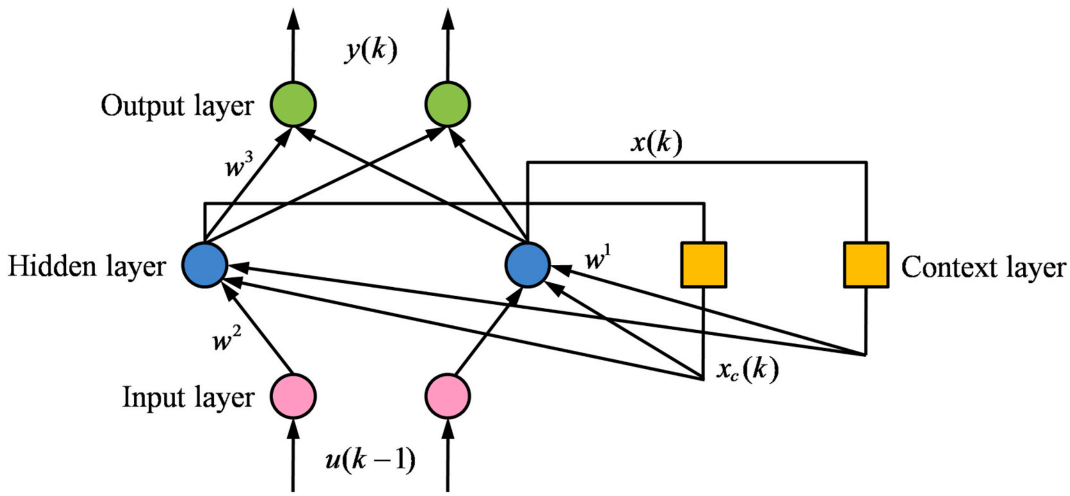

Fig. 3. Elman neural network structure diagram.

irradiance, irradiation duration, temperature, and relative humidity to construct the meteorological feature vector, as shown in Eq. (3):

$$X_i = [I_i, T_i, H_i, L_i] \tag{3}$$

where I_i is the average irradiance, T_i is the average temperature, H_i is the average relative humidity, L_i is the irradiation duration.

Accurate PV power prediction results are closely related to the selection of training samples. In order to select the training samples with higher correlation, historical data with high similarity are needed to make the prediction results more accurate. Similar days need to be selected according to the weather conditions, so the weather is divided into three categories: sunny days, cloudy days, and rainy days according to the amount of cloud covering.

Similar days are selected to find historical days with similar weather factors to the day to be predicted. The PV power of the similar days is taken as an input feature for the day to be predicted, and then the prediction is trained [47].

2.3.2. Elman neural network

The Elman neural network includes input layer, hidden layer, output layer, and context layer. Compared with BP neural network, there is an additional context layer, which can form local feedback and is a typical dynamic recurrent neural network [48]. The inclusion of this internal feedback makes the network have a memory function that can directly reflect the nonlinear and time-varying relationship between the PV output power and the impact factor. The structure of the Elman neural network used in this paper is shown in Fig. 3.

2.4. VMD for PV power generation

2.4.1. Mathematical model of VMD

VMD is a method of non-recursive variational mode decomposition of non-smooth signals, which can optimize a signal composed of multiple frequencies into several intrinsic mode functions (IMFs) of finite bandwidth using alternating multiplier methods. VMD decomposes a complex signal into k discrete sub-modes with different center frequencies. Each mode function converges around the center frequency ω_k and estimates the bandwidth of the frequency-shifted signal based on its Gaussian smoothness, thus minimizing the sum of the estimated bandwidths of each sub-mode.

If the original PV power P_{PV} is decomposed by VMD, several IMFs will be obtained. The sum of each IMF plus the residual r is equal to the P_{PV}. The mathematical model of the VMD algorithm process can be expressed by the constrained variational problem [26], as shown in Eq. (4):

$$\begin{cases} \min\limits_{\{u_k\},\{\omega_k\}} \left\{ \sum\limits_k \left\| \partial_t \left[\left(\delta(t) + \frac{j}{\pi t} \right) * u_k(t) \right] e^{-j\omega_k t} \right\|_2^2 \right\} \\ \text{s.t.} \sum\limits_k u_k(t) = f(t) \end{cases} \tag{4}$$

where ∂_t denotes the partial derivative with time t, $\delta(t)$ is the Dirac delta distribution, $\{u_k\}$ denotes the mode set $\{u_1, u_2, \ldots\ldots, u_k\}$, ω_k denotes the corresponding center frequency of the mode.

The quadratic penalty and augmented Lagrange multiplier are introduced to solve the constrained variational problem. The calculation formula is as shown in Eq. (5):

$$\begin{aligned} L(\{u_k\}, \{\omega_k\}, \lambda) = \alpha \sum_k \left\| \partial_t \left[\left(\delta(t) + \frac{j}{\pi t} \right) * u_k(t) \right] e^{-j\omega_k t} \right\|_2^2 \\ + \left\| f(t) - \sum_k u_k(t) \right\|_2^2 + \left\langle \lambda(t), f(t) - \sum_k u_k(t) \right\rangle \end{aligned} \tag{5}$$

where α is the penalty factor and $\lambda(t)$ is the Lagrange multiplier.

The alternate direction method of multipliers (ADMM) is adopted to iteratively update u_k^{n+1}, ω_k^{n+1}, λ_k^{n+1} to seek the optimal solution of Eq. (5).

$$\begin{aligned} L(\{u_k^{n+1}\}, \{\omega_k^{n+1}\}, \lambda_k^{n+1}) = \alpha \sum_k \left\| \partial_t \left[\left(\delta(t) + \frac{j}{\pi t} \right) * u_k^{n+1}(t) \right] e^{-j\omega_k^{n+1} t} \right\|_2^2 \\ + \left\| f(t) - \sum_k u_k^{n+1}(t) \right\|_2^2 + \left\langle \lambda_k^{n+1}(t), f(t) - \sum_k u_k^{n+1}(t) \right\rangle \end{aligned} \tag{6}$$

By using Fourier isometric transform, Eq. (6) is updated from the time domain to frequency domain and transformed into the form of non-negative frequency interval integral to obtain the subsequence and corresponding center frequency as shown in Eqs. (7) and (8):

$$\widehat{u}_k^{n+1}(\omega) = \frac{\widehat{f}(\omega) - \sum\limits_{i \neq k} \widehat{u}_i(\omega) + \frac{\widehat{\lambda}(\omega)}{2}}{1 + 2\alpha(\omega - \omega_k)^2} \tag{7}$$

$$\omega_k^{n+1} = \frac{\int_0^\infty \omega |\widehat{u}_k(\omega)|^2 d\omega}{\int_0^\infty |\widehat{u}_k(\omega)|^2 d\omega} \tag{8}$$

where $\widehat{u}_k^{n+1}(\omega)$, $\widehat{f}(\omega)$, $\widehat{\lambda}(\omega)$, $\widehat{u}_i(\omega)$ are the Fourier transforms of $u_k^{n+1}(\omega)$, $f(\omega)$, $\lambda(\omega)$ and $u_i(\omega)$ respectively.

The above iteration stops when the accuracy meets the requirement as shown in Eq. (9):

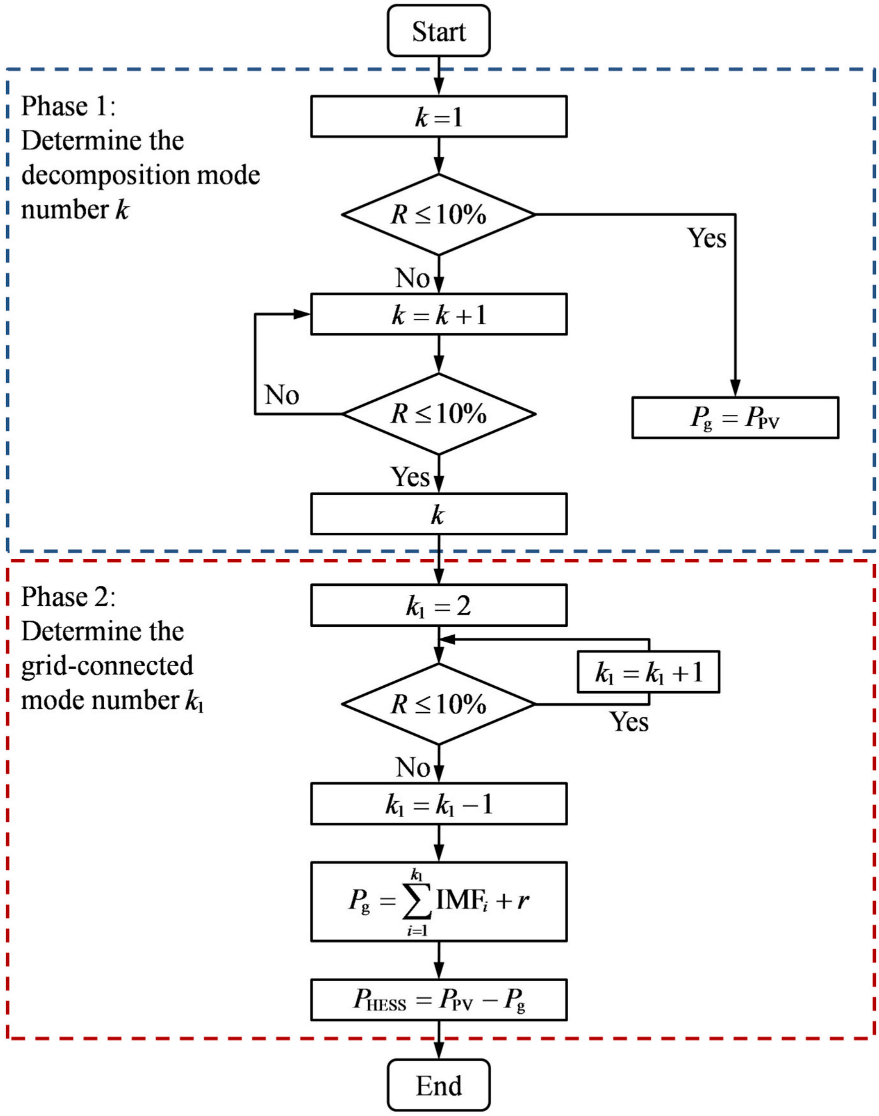

Fig. 4. VMD process for self-adaptive determination of k and k_1.

$$\sum_k \frac{\left\|\widehat{u}_k^{n+1} - \widehat{u}_k^n\right\|_2^2}{\left\|\widehat{u}_k^n\right\|_2^2} < \varepsilon \tag{9}$$

where ε is the given determination accuracy.

2.4.2. Control flow of VMD algorithm

The decomposition mode number k of the VMD algorithm is artificially determined and has great subjectivity. An unreasonable value of k can cause over-decomposition or under-decomposition of the original PV power, affecting the grid-connected effect. If the value of k is too small, the decomposed low-frequency signal will not meet the PV power fluctuation standard. If the value of k is too large, the HESS capacity will increase. The selection of grid-connected mode number k_1 is based on the grid-connected PV power fluctuation standard after k is determined. If the value of k_1 is too small, the capacity of HESS will increase. If the value of k_1 is too large, it will lead to unsatisfactory suppression of the target power.

Therefore, this paper proposes a self-adaptive VMD algorithm based on the active power variation requirement of the PV power station, which can determine the decomposition mode number k and the grid-connected mode number k_1 independently. It ensures grid-connected efficiency while obtaining a good decomposition result. The State Grid PV grid-connection standard stipulates that the PV active power variation for 1 min shall not exceed 10 % of the installed capacity [49]. Assume that the grid-connected PV power after being suppressed by HESS is P_g, the calculation formula of its fluctuation rate is as shown in Eq. (10):

$$R = \frac{maxP_g - minP_g}{P_{rated}} \times 100\% \tag{10}$$

where maxP_g is the maximum value of PV power over a period of time, minP_g is the minimum value of PV power over a period of time, P_{rated} is the installed PV capacity.

The VMD algorithm process based on the PV power fluctuation standard is shown in Fig. 4. It mainly includes two phases: determining the number of decomposition mode k and determining the number of grid-connected mode k_1, as follows:

Step 1: Perform VMD with the decomposition mode number $k = 1$ of the original PV power to judge whether the sub-mode IMF1 plus the residual r meets the requirements of the PV grid-connected fluctuation standard.

Step 2: If IMF1+r meets the fluctuation standard, the original PV power is directly connected to the grid.

Step 3: If IMF1+r does not meet the fluctuation standard, set the decomposition mode number $k = k + 1$ and deepen the decomposition cycle until it meets the fluctuation standard, then output k.
Step 4: Initialize the grid-connected mode number k_1 to 2, that is, connect the sub-modes IMF1 + IMF2+r to the grid and judge whether it meets the PV grid-connected fluctuation standard.
Step 5: If P_g meets the fluctuation standard, then $k_1 = k_1 + 1$, until the fluctuation standard is not met, then output k_1.
Step 6: If P_g does not meet the fluctuation standard, output $k_1 = k_1 - 1$. The difference between the original PV power P_{PV} and P_g is taken as the HESS power P_{HESS}, waiting for the next allocation.

3. HESS economic evaluation

3.1. Frequency characteristics of energy storage components

The working characteristics of lead-carbon batteries and supercapacitors are different. In order to facilitate the quantification of energy storage component characteristics and form a unified metric, the equivalent time (T_{ET}) is introduced [50], as shown in Eq. (11):

$$T_{ET} = \frac{E_s}{P_r} \tag{11}$$

where E_s is the rated capacity of the energy storage component, P_r is the rated power of the energy storage component.

T_{ET} is the time required to charge/discharge the energy storage component with rated power. The response time (T_T) is the time required for a complete charge/discharge cycle of the energy storage component, which is twice the equivalent time, i.e. $T_T = 2T_{ET}$.

The charging and discharging response time suitable for the energy storage component means that the energy storage component has high working efficiency and small life loss when it is normally charged and discharged during this period of time. The response frequency ω_T of the energy storage component is defined as shown in Eq. (12):

$$\omega_T = \frac{1}{T_T} \tag{12}$$

The response frequency and response time of the energy storage element are inversely proportional, and the response time is equal to twice the equivalent time. Therefore, energy storage element with large equivalent time is suitable for smoothing low frequency fluctuation, and energy storage element with small equivalent time is suitable for smoothing high frequency fluctuation. According to the characteristics of lead-carbon batteries and supercapacitors, the response time is from minutes to hours for lead-carbon batteries and milliseconds to minutes for supercapacitors [51]. Therefore, this paper uses the lead-carbon batteries to respond to the low-frequency fluctuation and the supercapacitors to respond to the high-frequency fluctuation.

3.2. Hilbert marginal spectrum based on VMD

From the principle of VMD and the determination of k and k_1 described in Section 3.1, it is assumed that the HESS power signal P_{HESS} is decomposed into $k - k_1$ intrinsic mode component u_k by VMD [52], as shown in Eq. (13):

$$P_{HESS} = \sum_{k=k_1+1}^{k} u_k(t) \tag{13}$$

The Hilbert transform is performed on each mode component u_k to obtain the instantaneous amplitude and frequency phase. Thus the Hilbert spectrum of each mode component is obtained according to the obtained instantaneous spectrum, as shown in Eq. (14):

$$H(u_k(t)) = \frac{1}{\pi}\int_{-\infty}^{+\infty} \frac{u_k(\tau)}{t-\tau} d\tau \tag{14}$$

According to Eq. (14), the analytic signal is constructed as Eq. (15) ~ Eq. (18):

$$z_k(t) = u_k(t) + jH(u_k(t)) = \alpha_k(t)e^{j\psi_k(t)} \tag{15}$$

$$\alpha_k(t) = \sqrt{u_k^2(t) + H^2(u_k(t))} \tag{16}$$

$$\psi_k(t) = arctan\frac{H(u_k(t))}{u_k(t)} \tag{17}$$

$$\omega_k(t) = \frac{d\psi_k(t)}{dt} \tag{18}$$

where $\alpha_k(t)$ is the instantaneous amplitude, $\psi_k(t)$ is the instantaneous phase, $\omega_k(t)$ is the instantaneous frequency of each mode component. The real part of the analytic signal in polar coordinate form is used as the Hilbert amplitude spectrum to describe the variation of the signal amplitude with time and frequency, as shown in Eq. (19):

$$H(\omega, t) = Re\left[\sum_{k=k_1+1}^{k} \alpha_k(t)exp\left(j\int \omega_k(t)dt\right)\right] \tag{19}$$

The Hilbert marginal spectrum is obtained by integrating Eq. (19) in time, as shown in Eq. (20). Statistically speaking, the marginal spectrum can indicate the distribution of the cumulative energy amplitude of the entire set of data at each frequency point and has a high-frequency resolution. This characteristic can be used as the basis for the power allocation of the HESS.

$$h(\omega) = \int_{-\infty}^{+\infty} H(\omega, t)dt \tag{20}$$

3.3. VHT applied to HESS capacity configuration

VHT (VMD-Hilbert) is a signal processing method that adaptively combines VMD with Hilbert transform. Through time integration, the marginal spectrum of each IMF can be obtained. Statistically speaking, the marginal spectrum can indicate the distribution of the cumulative energy amplitude of the entire set of data at each frequency point and has a high-frequency resolution. This characteristic can be used as the basis for the power allocation of the HESS.

Based on the physical properties of lead-carbon batteries and supercapacitors, a suitable dividing frequency ω_f should be found so that the mode IMF$_i$ and IMF$_{i+1}$ adjacent to ω_f are least mixed to achieve a reasonable power distribution within the HESS. Introduce the concept of signal energy. The signal energy method is a method that uses frequency to extract energy-based features from a signal [53]. The method is simple and quick to calculate. For a non-periodic signal, the instantaneous energy at a certain frequency is

$$E_k = \alpha^2{}_k{}^*\omega^2{}_k \tag{21}$$

where α_k is the instantaneous amplitude, ω_k is the instantaneous frequency.

If two IMFs have distinct amplitudes, but same frequency, then the mixing energy is

$$E_{mixing} = \alpha^2{}_i{}^*w^2{}_{mixing} + \alpha^2{}_{i+1}{}^*w^2{}_{mixing} \tag{22}$$

where α_i, α_{i+1} are instantaneous amplitudes corresponding to IMF$_i$ and IMF$_{i+1}$ respectively, ω_{mixing} is the frequency when IMFs mix.

In order to separate the low-frequency fluctuation component of the lead-carbon batteries and the high-frequency fluctuation component of

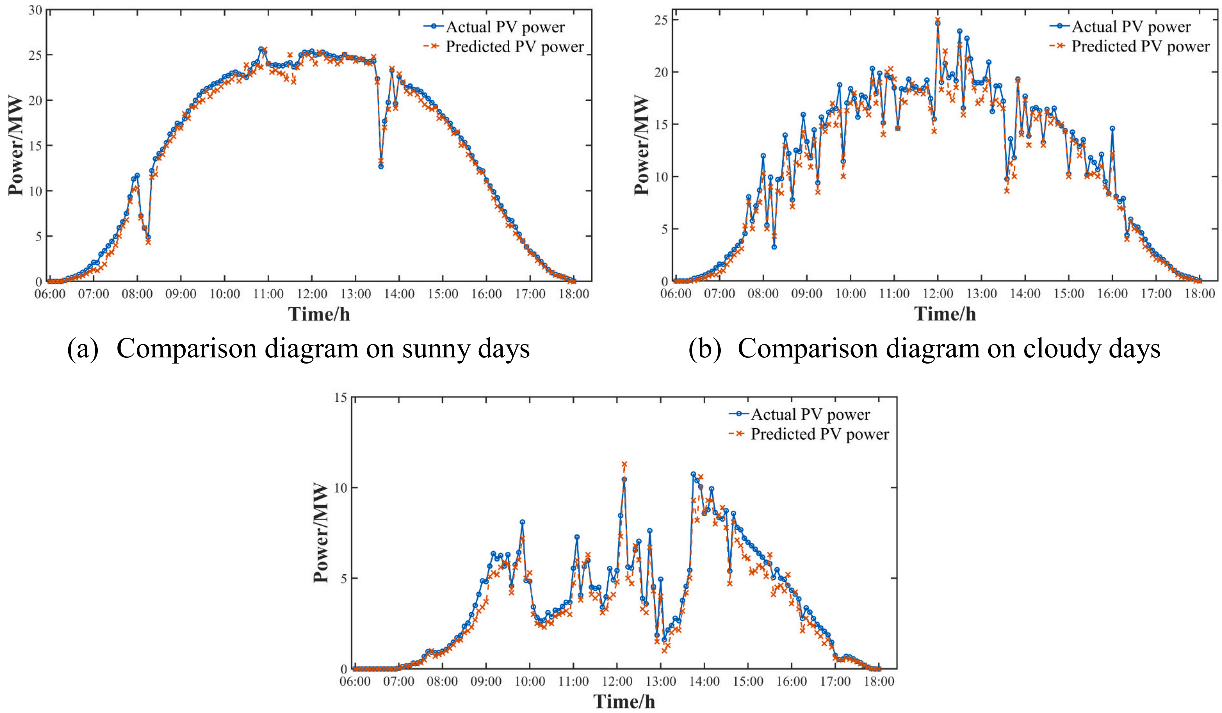

(a) Comparison diagram on sunny days

(b) Comparison diagram on cloudy days

(c) Comparison diagram on rainy days

Fig. 5. Comparison diagram of actual PV power and predicted PV power.

the supercapacitors with as little mixing as possible, the E_{mixing} has to be as small as possible. The frequency corresponding to the minimum E_{mixing} is the dividing frequency ω_f between high and low frequencies. Therefore, reconstruct the mode functions lower than ω_f and assign them to the lead-carbon batteries, and reconstruct the mode functions higher than ω_f and assign them to the supercapacitors, as shown in Eqs. (23) and (24):

$$P_{\mathrm{b}} = \sum_{i=k_1+1}^{f} \mathrm{IMF}_i \tag{23}$$

$$P_{\mathrm{c}} = \sum_{i=f+1}^{k} \mathrm{IMF}_i \tag{24}$$

3.4. HESS Economic Evaluation Model

This paper balances the smoothing effect of HESS on PV power fluctuation with economics. After fully considering the economic benefits in the process of HESS construction, operation, and maintenance, the HESS economic evaluation model is established. The lifecycle cost annualized model of HESS is calculated as shown in Eq. (25):

$$C_{\mathrm{HESS}} = C_{\mathrm{cap}} + C_{\mathrm{rep}} + C_{\mathrm{maint}} \tag{25}$$

(1) The initial investment cost of HESS is as shown in Eqs. (26) and (27):

$$C_{\mathrm{cap}} = \left(C_{\mathrm{bp}}P_{\mathrm{b}} + C_{\mathrm{be}}E_{\mathrm{b}} + C_{\mathrm{cp}}P_{\mathrm{c}} + C_{\mathrm{ce}}E_{\mathrm{c}}\right)\gamma_{\mathrm{CRF}} \tag{26}$$

$$\gamma_{\mathrm{CRF}} = \frac{\gamma(1+\gamma)^{T_{\mathrm{rt}}}}{(1+\gamma)^{T_{\mathrm{rt}}} - 1} \tag{27}$$

where C_{bp} and C_{be} are the cost per unit power and cost per unit capacity of lead-carbon batteries. C_{cp} and C_{ce} are the cost per unit power and cost per unit capacity of the supercapacitors. P_{b} and E_{b} are the power and capacity of the lead-carbon batteries. P_{c} and E_{c} are the power and capacity of the supercapacitors. γ is the discount rate of capital. T_{rt} is the life cycle of HESS.

(2) The replacement cost of HESS during the life cycle is as shown in Eq. (28):

$$C_{\mathrm{rep}} = \left[\left(C_{\mathrm{bp}}P_{\mathrm{b}} + C_{\mathrm{be}}E_{\mathrm{b}}\right)n_{\mathrm{b}} + \left(C_{\mathrm{cp}}P_{\mathrm{c}} + C_{\mathrm{ce}}E_{\mathrm{c}}\right)n_{\mathrm{c}}\right]\gamma_{\mathrm{CRF}} \tag{28}$$

where n_{b} and n_{c} are the replacement times of lead-carbon batteries and supercapacitors in the life cycle. Set the replacement time of supercapacitors to a fixed value according to experience. The number of lead-carbon batteries replacements is shown in Eq. (29):

$$n_{\mathrm{b}} = \mathrm{ceil}\left(T_{\mathrm{rt}}/T_{\mathrm{lifetime}} - 1\right) \tag{29}$$

where the function ceil(x) means to take the smallest integer not less than x.

(3) The maintenance cost of HESS is as shown in Eq. (30):

$$C_{\mathrm{maint}} = C_{\mathrm{b\_maint}}E_{\mathrm{b}} + C_{\mathrm{c\_maint}}E_{\mathrm{c}} \tag{30}$$

where $C_{\mathrm{b\_maint}}$ and $C_{\mathrm{c\_maint}}$ are the average annualized maintenance cost per unit capacity of lead-carbon batteries and supercapacitors respectively.

4. Example analysis

To demonstrate the real application of the proposed method in this paper, the actual operation data of a PV power station with an installed capacity of 30 MW is taken as an example for analysis. The sampling interval is 5 min and the sampling duration is 12 h from 6:00 am to 6:00 pm. This paper takes 10 %/5 min of the installed capacity as the smoothing target, which is more stringent than the State Grid PV grid-connection standard.

Table 3
The error statistics in different weather conditions.

Weather condition	RMSE/MW	MAPE/%
Sunny days	0.65	6.22
Cloudy days	0.92	12.71
Rainy days	0.61	11.92

Table 4
The values of k and k_1 in different weather conditions.

Weather condition	k	k_1
Sunny days	4	2
Cloudy days	5	1
Rainy days	3	1

4.1. PV power prediction case analysis

Select the actual operational and meteorological data (5-minute active power, total irradiance, scattered irradiance, temperature, and humidity) of the PV power station. Similar days are selected and the Elman neural network is used for the case analysis.

The root mean square error (RMSE) and mean absolute percentage error (MAPE) are selected to evaluate the PV power prediction results [54], as shown in Eqs. (31) and (32):

$$RMSE = \sqrt{\frac{1}{n}\sum_{n}\left(P_{\mathrm{i}} - P_{\mathrm{i}}^{*}\right)^{2}} \tag{31}$$

$$MAPE = \frac{1}{n}\sum_{n}\left|\frac{P_{\mathrm{i}} - P_{\mathrm{i}}^{*}}{P_{\mathrm{i}}}\right| \tag{32}$$

where P_{i} is the actual PV power, $P_{\mathrm{i}*}$ is the predicted PV power, n is the amount of data.

The comparison of the actual and predicted values of PV power in the three weather conditions is shown in Fig. 5. As can be seen from Fig. 5, Elman neural network model exhibits good prediction results.

The error statistics in different weather conditions are shown in Table 3.

As can be seen from Table 4, RMSE is within 1 MW and MAPE is within 13 % for all three weather conditions. On sunny days, the power changes gently and evenly, without sudden changes, so the prediction accuracy is the highest. Cloudy days and rainy days are less accurate than sunny days due to unstable weather conditions. In general, the prediction results are good in three weather conditions.

4.2. VMD of the original PV power in different weather conditions

The purpose of this paper is to configure energy storage for PV power station to smooth PV power fluctuation. The energy storage configuration scheme based on the worst scenario (i.e., the situation with the largest PV power fluctuation) can meet the energy storage requirements for various PV output scenarios. In order to verify the effectiveness of the proposed energy storage configuration strategy, this paper selects the PV power curves with maximum fluctuation in three typical weather conditions: sunny days, cloudy days, and rainy days. The original PV power curves in three weather conditions are shown in Fig. 6.

By performing self-adaptive VMD of the original PV power, the grid-connected PV power that meets the fluctuation standard can be obtained. The original PV power is decomposed by VMD into the corresponding IMFs and r, as shown in Fig. 7.

From Fig. 7, it can be seen that the decomposition mode number k differs in different weather conditions. The values of k and k_1 in different weather conditions are shown in Table 4. On sunny days, light conditions change smoothly, the PV power changes less frequently. Through VMD of the original PV power, $k = 4$ and $k_1 = 2$ can be obtained so as to meet the fluctuation standard of grid-connected PV power. On cloudy days, the PV power changes more frequently and dramatically due to frequently changing meteorological factors such as cloud movement, $k = 5$ and $k_1 = 1$ can be obtained. On rainy days, the overall power generated is not high due to insufficient light conditions, the PV power changes less frequently, $k = 3$ and $k_1 = 1$ can be obtained. Each IMF has

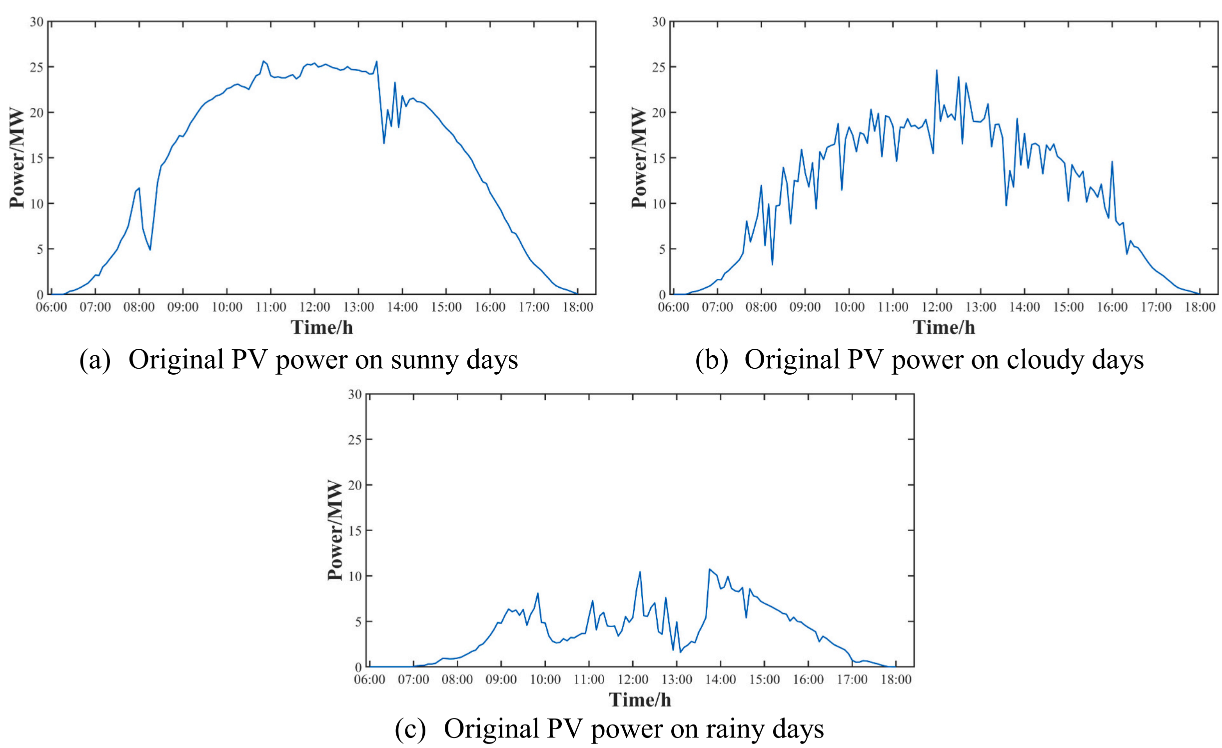

Fig. 6. Original PV power in different weather conditions.

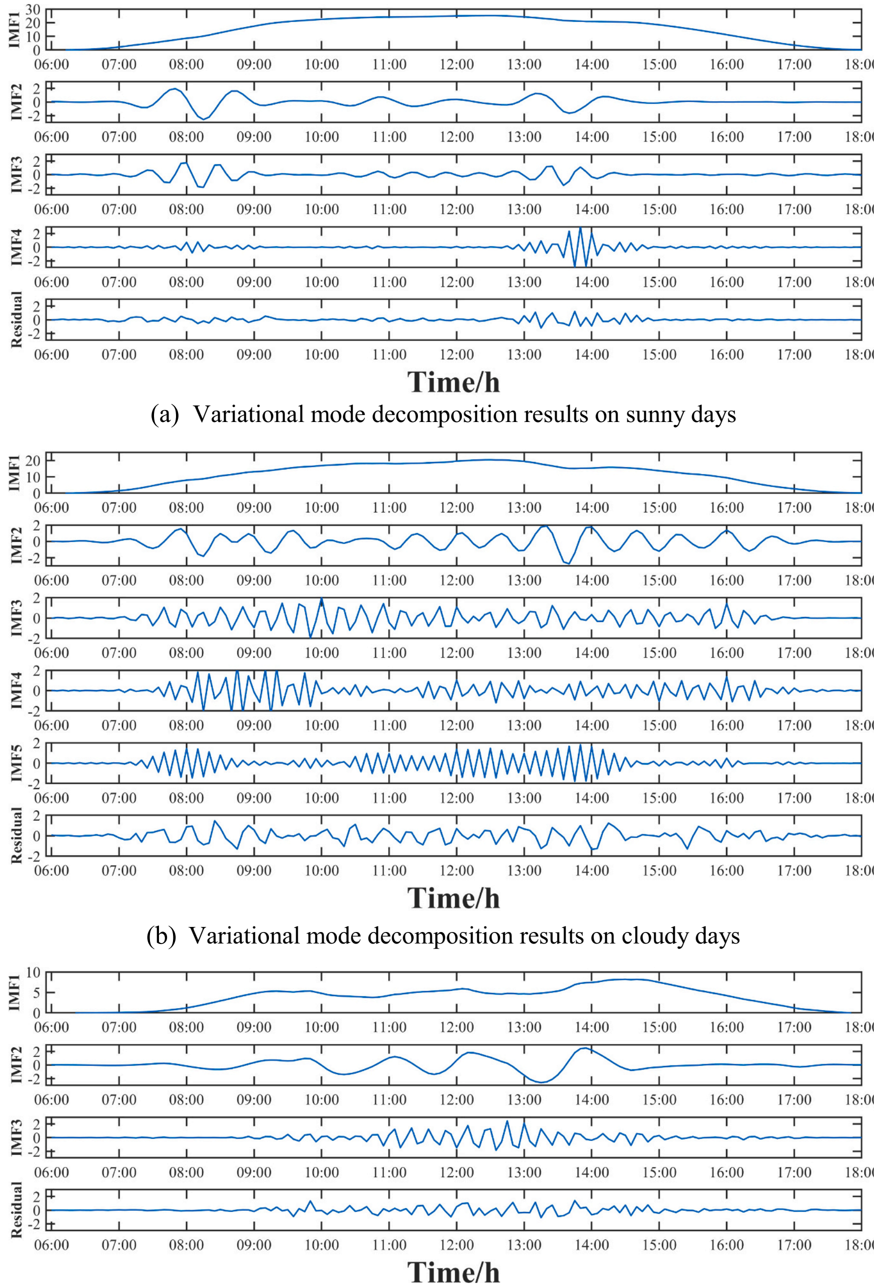

(a) Variational mode decomposition results on sunny days

(b) Variational mode decomposition results on cloudy days

(c) Variational mode decomposition results on rainy days

Fig. 7. Variational mode decomposition results.

different fluctuations. IMF1 is a smooth curve without multiple peaks and valleys. The fluctuation of the mode components increases with the increase of the sub-mode order and the number of peaks and valleys also increases.

4.3. Analysis of PV power fluctuation smoothing effect

Compare the grid-connected PV power with the original PV power in three weather conditions, the result is shown in Fig. 8. As can be seen in Fig. 8, the grid-connected power curve is relatively smooth after VMD, which can characterize the overall trend of the original power signal. Relative to the original PV power, after the HESS compensation, grid-connected PV power fluctuation has significantly reduced, reflecting the effect of the HESS to smooth the PV power fluctuation. When the original PV power rises suddenly, the HESS absorbs energy to slow down the rise in power, when the original PV power falls suddenly, the HESS releases energy to slow down the fall in power, thus reducing the fluctuation of the PV power. Taking sunny days for example, if the self-adaptive VMD algorithm is not used, then $k_1 = 1$. Compare the HESS power with different k_1 on sunny days, the result is shown in Fig. 9. The power taken up by the HESS is 5.07 MW for $k_1 = 1$ and 4.19 MW for $k_1 = 2$, a reduction of 17.36 %. This shows that the optimization of k_1 satisfies the PV power fluctuation rate requirement and reduces the HESS capacity configuration.

Fig. 10 shows the 5 min PV power fluctuation rate curve before and after smoothing. It can be seen that the original PV power fluctuates frequently, the maximum fluctuation rate on sunny, cloudy, and rainy days are 16.50 %/5 min, 30.49 %/5 min, and 17.69 %/5 min respectively. The maximum fluctuation rate is higher than the upper limit of 10 %/5 min grid-connected fluctuation rate standard in all three

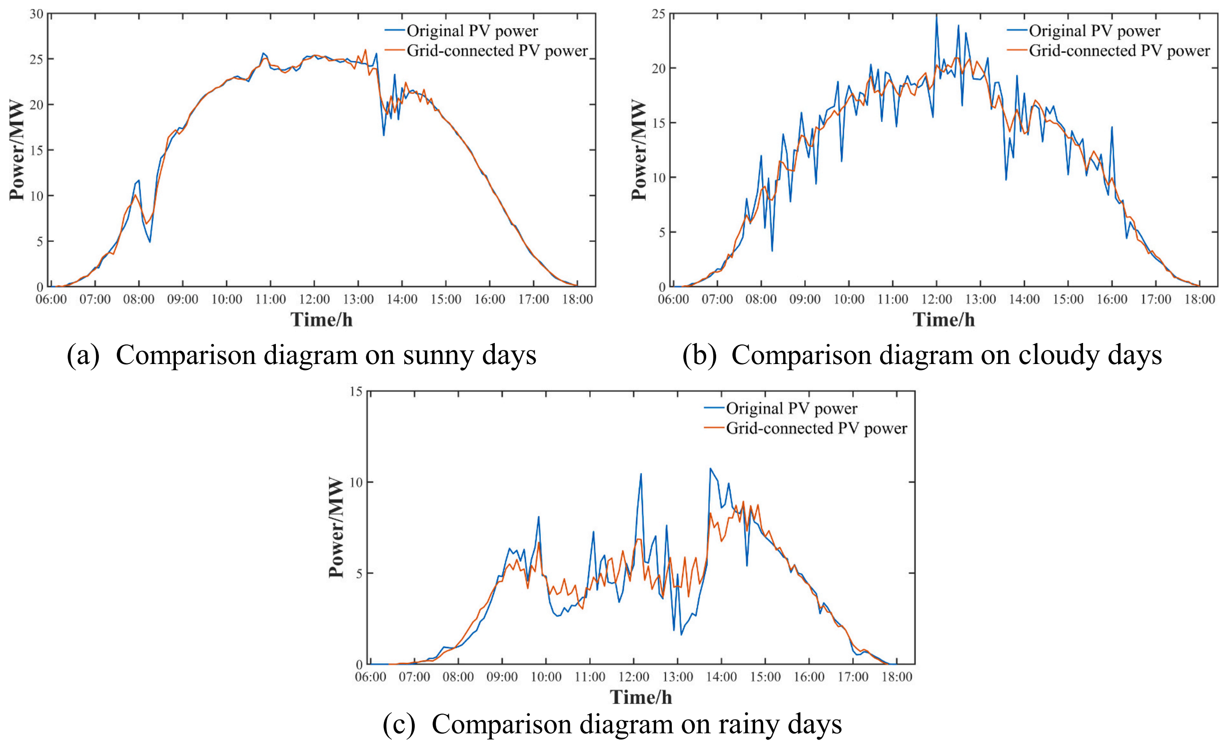

Fig. 8. Comparison diagram of original PV power and grid-connected PV power.

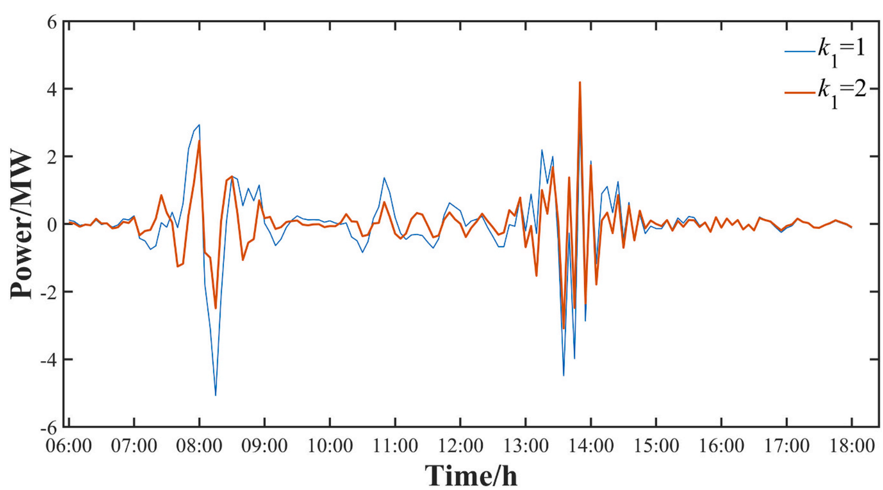

Fig. 9. Comparison diagram of HESS power with different k_1 on sunny days.

weather conditions. After the original PV power is smoothed by the HESS, the fluctuation rate of grid-connected PV power drops significantly. The maximum fluctuation rate of grid-connected PV power after self-adaptive VMD in three weather conditions are 9.68 %/5 min, 9.49 %/5 min, and 8.19 %/5 min, which meet the PV grid-connected fluctuation standard. Thus, the effectiveness of the smoothing strategy is verified.

The simulation results show that the self-adaptive VMD algorithm proposed in this paper can independently select k and k_1 according to different PV output characteristics, which overcomes the shortcomings of the existing VMD algorithm such as poor self-adaptive ability and avoids over-decomposition or under-decomposition caused by subjectively setting the decomposition scale. Meanwhile, the self-adaptive determination of k_1 maximizes the grid-connected PV power while meeting the grid-connected fluctuation rate standard, overcoming the disadvantages of the existing VMD algorithm scenarios such as poor adaptive capability, significantly enhance the applicability of such method. Moreover, the smoothing effect of this paper is also better than that of the EMD algorithm [55].

4.4. HESS power distribution analysis

The following analysis is for the cloudy days with the largest PV power fluctuation rate. The role of HESS in PV power smoothing is to compensate the difference power between original PV power and grid-connected PV power (total power of IMF2 ~ IMF5). IMF2 ~ IMF5 is assigned to HESS to compensate. The output power of HESS is shown in Fig. 11.

The VMD-Hilbert method is used to decompose the HESS power. As shown in Fig. 12, the marginal spectrum is obtained by integrating the

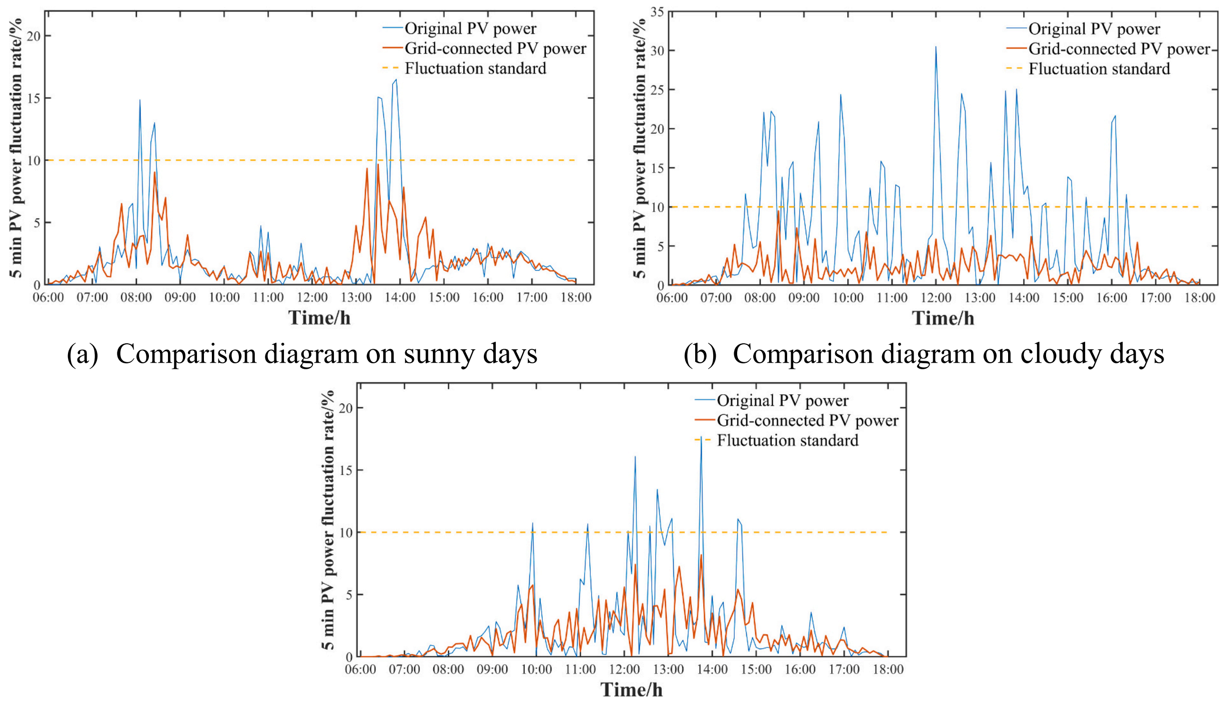

(a) Comparison diagram on sunny days

(b) Comparison diagram on cloudy days

(c) Comparison diagram on rainy days

Fig. 10. Comparison diagram of original PV power and grid-connected PV power fluctuation rate.

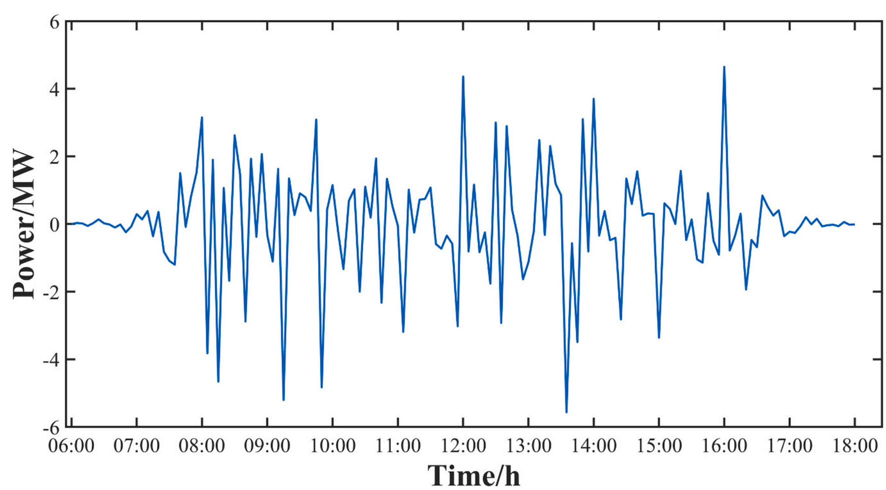

Fig. 11. Output power of HESS on cloudy days.

time based on the VHT method. This method can separate the signals of different frequencies and distinguish the high and low frequencies for power distribution to the HESS. The dividing frequency corresponding to the smallest mode mixing energy is calculated to be 2×10^{-3}Hz. Therefore, 2×10^{-3}Hz is chosen as the charge/discharge response frequency divider for lead-carbon batteries and supercapacitors, which corresponds to a response time of 500 s. The signal above this frequency dividing point is assigned to the supercapacitors, while the signal below this frequency dividing point is assigned to the lead-carbon batteries. That is, IMF2 ~ IMF3 are assigned to lead-carbon batteries and IMF4 ~ IMF5 are assigned to supercapacitors. Such a distribution satisfies the charge/discharge response frequencies of lead-carbon batteries and the supercapacitors. The power distribution of lead-carbon batteries and supercapacitors is shown in Fig. 13. From Fig. 13, it can be seen that the lead-carbon battery with higher energy density bears lower power frequency and longer charging and discharging durations. The supercapacitor with higher responsiveness assumes higher power frequency, the charge and discharge states change rapidly. The power distribution is consistent with the response characteristics of lead-carbon batteries and supercapacitors.

4.5. Calculation of HESS life cycle annualized cost

In order to compare the capacity configuration of self-adaptive VMD and EMD for HESS and the economic advantages of HESS compared with a single lead-carbon battery energy storage system, three configuration schemes are selected. Scheme 1 is a single lead-carbon battery energy storage system, Scheme 2 is a HESS based on the EMD, Scheme 3 is a HESS based on the self-adaptive VMD. The related parameters of HESS capacity programming are shown in Table 5. The comparison of

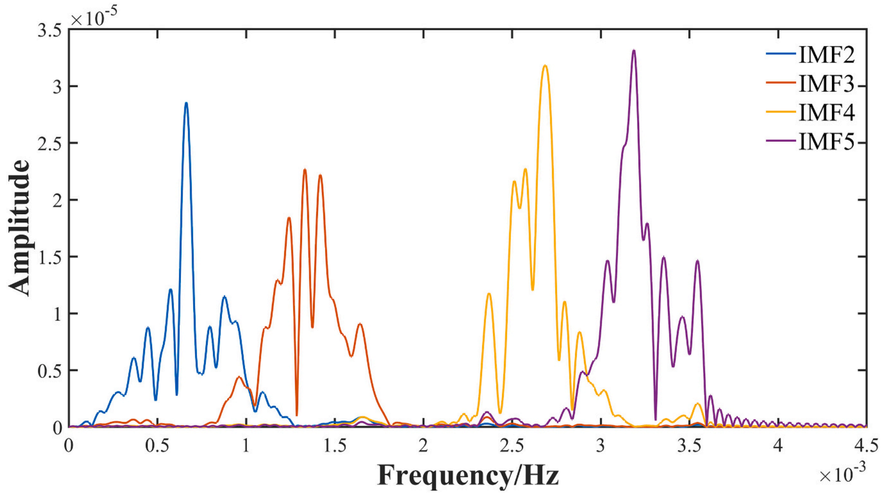

Fig. 12. Marginal spectrum obtained by VHT on cloudy days.

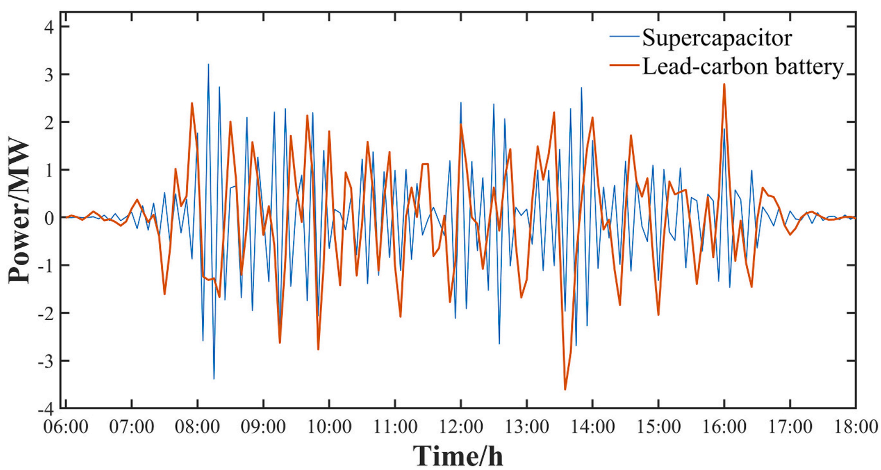

Fig. 13. Internal power distribution of HESS on cloudy days.

Table 5
Related parameters of HESS capacity programming.

Parameters	Unit	Lead-carbon battery	Supercapacitor
Power unit price	USD/MW	437,000	218,000
Capacity unit price	USD/MWh	93,600	4,214,700
Annualized maintenance cost	USD/MWh	7,800	7,800
SOC threshold	–	0.3–0.8	0.1–0.9
Discount rate of funds	–	0.05	
Lifecycle	a	20	

Table 6
Comparison of calculative results among three energy storage configuration schemes.

Parameters	Unit	Scheme 1	Scheme 2	Scheme 3
E_b	MWh	1.56	1.43	1.18
P_b	MW	4.89	3.14	2.85
E_c	MWh	–	0.23	0.17
P_c	MW	–	3.82	3.41
Lead-carbon battery service life	a	2.93	4.76	5.22
Annualized cost of energy storage system	1,000 USD	651.39	458.32	344.26

calculative results among three energy storage configuration schemes is shown in Table 6.

To verify the effectiveness of the HESS compared to a single lead-carbon battery energy storage system, Scheme 1 and Scheme 3 are selected for analysis. From Table 6, it can be seen that the power and capacity configurations of energy storage can be reduced by using HESS. The capacity configuration of lead-carbon battery storage in HESS is reduced by 24.36 % and the power configuration is reduced by 41.72 % relative to single lead-carbon battery storage; the annualized cost of HESS is reduced by 47.15 % relative to single lead-carbon battery storage system. This is because Scheme 1 only has lead-carbon batteries installed in the energy storage system to smooth PV power fluctuation. The batteries need to be charged and discharged frequently. They have a service life of 2.93 years, so they need to be replaced 6 times during their life cycle. When the HESS based on self-adaptive VMD proposed in this paper is used, the service life of lead-carbon batteries is 5.22 years and they only need to be replaced 3 times during their life cycle. The ability of the HESS to effectively extend the service life of the lead-carbon battery is the main influence factor for the annualized cost reduction.

To verify the effectiveness of self-adaptive VMD compared to EMD, Scheme 2 and Scheme 3 are selected for analysis. From Table 6, it can be seen that compared to EMD, self-adaptive VMD can reduce the capacity and power configuration of the HESS. The capacity configuration of lead-carbon batteries decreased by 17.48 % and the power configuration decreased by 9.24 %; They have a service life of 4.76 years, so they need to be replaced 4 times during their life cycle. The capacity configuration of supercapacitors decreased by 26.09 % and the power configuration decreased by 10.73 %.The annualized cost of self-adaptive VMD is reduced by 24.89 % compared to EMD. This is because the self-adaptive VMD avoids the mode mixing problem caused by EMD and makes full use of the complementary characteristics of the lead-carbon batteries and supercapacitors when configuring HESS capacity, thus reducing the annualized cost.

In summary, compared with the other schemes, the configuration method of Scheme 3 based on self-adaptive VMD proposed in this paper has the smallest comprehensive configuration capacity, the longest service life of lead-carbon batteries, the smallest annualized cost, and the best comprehensive economic benefits. The scheme can provide a reference for the practical PV stabilization strategy formulation.

5. Conclusion

The HESS has been widely studied and applied worldwide for smoothing PV power fluctuation to enable stable grid operation. However, the algorithms currently used in HESS are not effective in smoothing PV power fluctuation and are less economical, which is considered as one of their main drawbacks. This paper proposes a HESS smoothing PV power fluctuation method based on self-adaptive VMD. The main work and conclusions are as follows:

The self-adaptive VMD method proposed in this paper can determine the smoothing strategy according to different weather conditions. The decomposition mode number of the VMD and the grid-connected mode number are effectively determined under the premise of ensuring the maximum PV power fluctuation rate limit. With this algorithm, the excessive capacity of HESS is avoided, thus realizing the self-adaptability of smoothing PV power fluctuation.

Smoothing PV power fluctuation requires accurate PV power prediction. In this paper, a PV power prediction method is proposed. In all three weather conditions, RMSE is within 1 MW and MAPE is within 13 %, indicating good prediction results.

In order to give full play to the advantages of lead-carbon batteries and supercapacitors, VMD-Hilbert is used to decompose the HESS power. A method to determine the dividing frequency based on the minimum mode mixing energy is proposed, so that the frequency dividing point is determined by the marginal spectrum. The HESS power is divided into high-frequency and low-frequency parts and used as the power of the lead-carbon batteries and supercapacitors to obtain the energy storage capacity configuration. The reasonable allocation of capacity can extend the service life of HESS while meeting the PV grid-connected fluctuation standard.

HESS economic evaluation model is established and HESS life cycle annualized cost is analyzed. The results indicate that the maximum value of 5 min power fluctuation rate in different weather conditions after VMD is 9.68 %, 9.49 %, and 8.19 % respectively, which meets the PV grid-connected fluctuation standard. Due to the optimization of k_1, the power of HESS can be reduced by 17.36 % on sunny days compared to the conventional VMD. The HESS life cycle annualized cost in the maximum fluctuation weather condition with the application of self-adaptive VMD is 344,264 US dollars, which decreases 24.89 % compared with EMD.

CRediT authorship contribution statement

Gang Xiao: Writing – original draft, Formal analysis. **Fen Xu:** Writing – original draft, Software. **Lianghuai Tong:** Writing – review & editing. **Haoran Xu:** Validation. **Peiwang Zhu:** Conceptualization, Writing – review & editing.

Declaration of competing interest

We declare that we have no financial and personal relationships with other people or organizations that can inappropriately influence our work, there is no professional or other personal interest of any nature or kind in any product, service and/or company that could be construed as influencing the position presented in, or the review of, the manuscript entitled.

Data availability

The data that has been used is confidential.

Acknowledgement

The authors gratefully acknowledge the support from the Zhejiang Provincial Natural Science Foundation (NO. LR20E060001) and the Zhejiang Provincial Key R&D Program (NO. 2022C01043).

References

[1] T. Yao, J. Wang, H. Wu, P. Zhang, S. Li, Y. Wang, et al., A photovoltaic power output dataset: multi-source photovoltaic power output dataset with python toolkit, Sol. Energy 230 (2021) 122–130, https://doi.org/10.1016/j.solener.2021.09.050.

[2] M. Anvari, B. Werther, G. Lohmann, M. Wächter, J. Peinke, H.-P. Beck, Suppressing power output fluctuations of photovoltaic power plants, Sol. Energy 157 (2017) 735–743, https://doi.org/10.1016/j.solener.2017.08.038.

[3] S. Rahman, S. Saha, M.E. Haque, S.N. Islam, M.T. Arif, M. Mosadeghy, et al., A framework to assess voltage stability of power grids with high penetration of solar PV systems, Int. J. Electr. Power Energy Syst. 139 (2022), 107815, https://doi.org/10.1016/j.ijepes.2021.107815.

[4] S. Sukumar, M. Marsadek, K.R. Agileswari, H. Mokhlis, Ramp-rate control smoothing methods to control output power fluctuations from solar photovoltaic (PV) sources-a review, J. Energy Storage 20 (2018) 218–229, https://doi.org/10.1016/j.est.2018.09.013.

[5] Q. Peng, A. Sangwongwanich, Y. Yang, F. Blaabjerg, Grid-friendly power control for smart photovoltaic systems, Sol. Energy 210 (2020) 115–127, https://doi.org/10.1016/j.solener.2020.05.001.

[6] M.J.E. Alam, K.M. Muttaqi, D. Sutanto, A novel approach for ramp-rate control of solar PV using energy storage to mitigate output fluctuations caused by cloud passing, IEEE Trans. Energy Convers. 29 (2014) 507–518, https://doi.org/10.1109/TEC.2014.2304951.

[7] X. Liu, Research on optimal dispatch method of virtual power plant considering various energy complementary and energy low carbonization, Int. J. Electr. Power Energy Syst. 136 (2022), 107670, https://doi.org/10.1016/j.ijepes.2021.107670.

[8] K.R. Khalilpour, A. Vassallo, A generic framework for distributed multi-generation and multi-storage energy systems, Energy 114 (2016) 798–813, https://doi.org/10.1016/j.energy.2016.08.029.

[9] R. Xiong, Y. Duan, J. Cao, Q. Yu, Battery and ultracapacitor in-the-loop approach to validate a real-time power management method for an all-climate electric vehicle, Appl. Energy 217 (2018) 153–165, https://doi.org/10.1016/j.apenergy.2018.02.128.

[10] A. Abbassi, M.A. Dami, M. Jemli, A statistical approach for hybrid energy storage system sizing based on capacity distributions in an autonomous PV/Wind power generation system, Renew.Energy 103 (2017) 81–93, https://doi.org/10.1016/j.renene.2016.11.024.

[11] J.C. Hernández, M. Gomez-Gonzalez, F. Sanchez-Sutil, F. Juradob, Optimization of battery/supercapacitor-based photovoltaic household-prosumers providing self-consumption and frequency containment reserve as influenced by temporal data granularity, J. Energy Storage 36 (2021), 102366, https://doi.org/10.1016/j.est.2021.102366.

[12] P.T. Moseley, D.A.J. Rand, K. Peters, Enhancing the performance of lead–acid batteries with carbon – in pursuit of an understanding, J. Power Sources 295 (2015) 268–274, https://doi.org/10.1016/j.jpowsour.2015.07.009.

[13] M. Saravanan, P. Sennu, M. Ganesan, S. Ambalavanan, Multi-walled carbon nanotubes percolation network enhanced the performance of negative electrode for lead-acid battery, J. Electrochem. Soc. 160 (2013) A70–A76, https://doi.org/10.1149/2.062301jes.

[14] S.M. Kumar, S. Arun, S. Mayavan, Effect of carbon nanotubes with varying dimensions and properties on the performance of lead acid batteries operating under high rate partial state of charge conditions, J. Energy Storage 24 (2019), 100806, https://doi.org/10.1016/j.est.2019.100806.

[15] A.G. Olabi, Q. Abbas, A.A. Makky, M.A. Abdelkareem, Supercapacitors as next generation energy storage devices: properties and applications, Energy 248 (2022), 123617, https://doi.org/10.1016/j.energy.2022.123617.

[16] L. Wang, Y. Gao, Design of hybrid energy storage system control strategy to suppress output fluctuations of photovoltaic generation system, Electr.Meas. Instrum. 52 (2015) 49–54, https://doi.org/10.1109/CMPSAC.1995.524810.

[17] M. Ding, J. Wu, A novel control strategy of hybrid energy storage system for wind power smoothing, Electr. Power Compon. Syst. 45 (2017) 1265–1274, https://doi.org/10.1080/15325008.2017.1346004.
[18] Y. Zhou, Z. Yan, N. Li, A novel state of charge feedback strategy in wind power smoothing based on short-term forecast and scenario analysis, IEEE Trans. Sustain. Energy 8 (2017) 870–879, https://doi.org/10.1109/TSTE.2016.2625305.
[19] Z. Wu, X. Jiang, H. Ma, S. Ma, Wavelet packet-fuzzy control of hybrid energy storage systems for PV power smoothing, Proc.CSEE 34 (2014) 317–324, https://doi.org/10.13334/j.0258-8013.pcsee.2014.03.001.
[20] C. Tian, K. Li, Y. Yan, C. Zhang, A multi-time scale control strategy of hybrid energy storage system in wind farm based on empirical mode decomposition, Power Syst. Technol. 39 (2015) 2167–2172, https://doi.org/10.13335/j.1000-3673.pst.2015.08.016.
[21] Z. He, Q. Wang, Y. Shen, M. Sun, Kernel sparse multitask learning for hyperspectral image classification with empirical mode decomposition and morphological wavelet-based features, IEEE Trans. Geosci. Remote Sens. 52 (2014) 5150–5163, https://doi.org/10.1109/TGRS.2013.2287022.
[22] M. Sanabria-Villamizar, M. Bueno-López, J.C. Hernández, D. Vera, Characterization of household-consumption load profiles in the time and frequency domain, Int. J. Electr. Power Energy Syst. 37 (2022), 107756, https://doi.org/10.1016/j.ijepes.2021.107756.
[23] F. Sánchez-Sutil, J.C. Hernández, A. Cano, C.R. Baier, Influence of data sampling frequency on household consumption load profile features: a case study in Spain, Sensors 20 (2020) 6034, https://doi.org/10.3390/s20216034.
[24] C. Wang, H. Zhang, W. Fan, P. Ma, A new chaotic time series hybrid prediction method of wind power based on EEMD-SE and full-parameters continued fraction, Energy 138 (2017) 977–990, https://doi.org/10.1016/j.energy.2017.07.112.
[25] Y. Jia, J. Zheng, H. Chen, Z. Yan, J. Wang, X. Chang, Capacity allocation optimization of energy storage in thermal-storage frequency regulation dispatch system based on EEMD, Power Syst.Technol. 42 (2018) 2930–2937, https://doi.org/10.13335/j.1000-3673.pst.2018.0964.
[26] K. Dragomiretskiy, D. Zosso, Variational mode decomposition, IEEE Trans. Signal Process. 62 (2014) 531–544, https://doi.org/10.1109/TSP.2013.2288675.
[27] C. Park, C. Kim, Y. Choi, S. Won, Y. Moriyoshi, The influences of hydrogen on the performance and emission characteristics of a heavy duty natural gas engine, Int. J. Hydrog. Energy 36 (2011) 3739–3745, https://doi.org/10.1016/j.ijhydene.2010.12.021.
[28] P.D. Achlerkar, S.R. Samantaray, M.S. Manikandan, Variational mode decomposition and decision tree based detection and classification of power quality disturbances in grid-connected distributed generation system, IEEE Trans Smart Grid 9 (2018) 3122–3132, https://doi.org/10.1109/TSG.2016.2626469.
[29] Q. Zhang, J. Wu, Y. Ma, G. Li, J. Ma, C. Wang, Short-term load forecasting method with variational mode decomposition and stacking model fusion, Sustain. EnergyGrids Netw. 30 (2022), 100622, https://doi.org/10.1016/j.segan.2022.100622.
[30] J. Naik, S. Dash, P.K. Dash, R. Bisoi, Short term wind power forecasting using hybrid variational mode decomposition and multi-kernel regularized pseudo inverse neural network, Renew.Energy 118 (2018) 180–212, https://doi.org/10.1016/j.renene.2017.10.111.
[31] A. Tulsyan, Y. Tsai, R.B. Gopaluni, R.D. Braatz, State-of-charge estimation in lithium-ion batteries: a particle filter approach, J. Power Sources 331 (2016) 208–233, https://doi.org/10.1016/j.jpowsour.2016.08.113.
[32] R. Amirante, E. Cassone, E. Distaso, P. Tamburrano, Overview on recent developments in energy storage: mechanical, electrochemical and hydrogen technologies, Energy Convers. Manag. 132 (2017) 372–387, https://doi.org/10.1016/j.enconman.2016.11.046.
[33] B. Bozkaya, J. Settelein, M. Komma, G. Gryglewicz, G. Sextl, G.A. Giffin, Influence of basic carbon additives on the electrochemical performance of lead-carbon batteries, J. Energy Storage 44 (2021), 103400, https://doi.org/10.1016/j.est.2021.103400.
[34] B. Gao, X. Liu, Z. Zhu, A bottom-up model for household load profile based on the consumption behavior of residents, Energies 11 (2018) 2112, https://doi.org/10.3390/en11082112.
[35] R. Stierle, E. Sauer, J. Eller, M. Theiss, P. Rehner, P. Ackermann, et al., Guide to efficient solution of PC-SAFT classical density functional theory in various coordinate systems using fast Fourier and similar transforms, Fluid Phase Equilib. 504 (2020), 112306, https://doi.org/10.1016/j.fluid.2019.112306.
[36] C. Mateo, J.A. Talavera, Short-time Fourier transform with the window size fixed in the frequency domain, Digit.Signal Process. 77 (2018) 13–21, https://doi.org/10.1016/j.dsp.2017.11.003.
[37] M.A. Rodríguez, J.L.S. Emeterio, J.C. Lázaro, A. Ramos, Ultrasonic flaw detection in NDE of highly scattering materials using wavelet and Wigner-Ville transform processing, Ultrasonics 42 (2004) 847–851, https://doi.org/10.1016/j.ultras.2004.01.063.
[38] M.S. Imani, M.A. Imani, A. Soltani, F. Shamac, Miniaturized microstrip suppressing lowpass cell for hybrid applications, AEU-Int. J. Electron. Commun. 136 (2021), 153734, https://doi.org/10.1016/j.aeue.2021.153734.
[39] M. Santhosh, C. Venkaiah, D. Kumar, Ensemble empirical mode decomposition based adaptive wavelet neural network method for wind speed prediction, Energy Convers. Manag. 168 (2018) 482–493, https://doi.org/10.1016/j.enconman.2018.04.099.
[40] X. Zha, P. Wang, F. Liu, J. Gong, F. Zhu, Segmented power distribution control system based on hybrid cascaded multilevel converter with parts of energy storage, IET Power Electron. 10 (2018) 2076–2084, https://doi.org/10.1049/iet-pel.2016.0943.
[41] S. Kaplanis, E. Kaplani, J.K. Kaldellis, PV temperature and performance prediction in free-standing, BIPV and BAPV incorporating the effect of temperature and inclination on the heat transfer coefficients and the impact of wind, efficiency and ageing, Renew.Energy 181 (2022) 235–249, https://doi.org/10.1016/j.renene.2021.08.124.
[42] M. Talha, S.R.S. Raihan, N.A. Rahim, PV inverter with decoupled active and reactive power control to mitigate grid faults, Renew.Energy 162 (2020) 877–892, https://doi.org/10.1016/j.renene.2020.08.067.
[43] M.F. Roslan, M.A. Hannan, P.J. Ker, R.A. Begum, T.I. Mahlia, Z.Y. Dong, Scheduling controller for microgrids energy management system using optimization algorithm in achieving cost saving and emission reduction, Appl. Energy 292 (2021), 116883, https://doi.org/10.1016/j.apenergy.2021.116883.
[44] J. Adhikari, I.V. Prasanna, S.K. Panda, Power conversion system for high altitude wind power generation with medium voltage AC transmission, Renew.Energy 93 (2016) 562–578, https://doi.org/10.1016/j.renene.2016.03.004.
[45] K. Okay, S. Eray, A. Eray, Development of prototype battery management system for PV system, Renew.Energy 181 (2022) 1294–1304, https://doi.org/10.1016/j.renene.2021.09.118.
[46] F. Naseri, S. Karimi, E. Farjah, E. Schaltz, Supercapacitor management system: a comprehensive review of modeling, estimation, balancing, and protection techniques, Renew. Sustain. Energy Rev. 155 (2022), 111913, https://doi.org/10.1016/j.rser.2021.111913.
[47] Y. Zhou, N. Zhou, L. Gong, M. Jiang, Prediction of photovoltaic power output based on similar day analysis, genetic algorithm and extreme learning machine, Energy 204 (2020), 117894, https://doi.org/10.1016/j.energy.2020.117894.
[48] H. Jia, B. Taheri, Model identification of solid oxide fuel cell using hybrid Elman neural network/quantum pathfinder algorithm, Energy Rep. 7 (2021) 3328–3337, https://doi.org/10.1016/j.egyr.2021.05.070.
[49] State Grid Corporation of China, Technical Rule for Connecting Photovoltaic Power Station to Power Grid: Q/GDW 1617–2015, China Electric Power Press, Beijing, 2016.
[50] L. Cheng, F. Zhang, M. Xie, Y. Wang, H. Zou, High power density optimal configuration for hybrid energy storage system based on equivalent time, Acta Aeronaut.Astronaut.Sin. 38 (2018), 322129, https://doi.org/10.7527/S1000-6893.2018.22129.
[51] H. Chen, T.N. Cong, W. Yang, C. Tan, Y. Li, Y. Ding, Progress in electrical energy storage system: a critical review, Prog. Nat. Sci. 19 (2009) 291–312, https://doi.org/10.1016/j.pnsc.2008.07.014.
[52] J.N. Yang, Y. Lei, S. Pan, N. Huang, System identification of linear structures based on Hilbert-Huang spectral analysis. Part 1: normal modes, Earthq. Eng. Struct. Dyn. 32 (2003) 1443–1467, https://doi.org/10.1002/eqe.287.
[53] R. Yadav, A.K. Pradhan, I. Kamwa, Real-time multiple event detection and classification in power system using signal energy transformations, IEEE Trans. Ind. Inform. 15 (2019) 1521–1531, https://doi.org/10.1109/TII.2018.2855428.
[54] I.O. Nour-eddine, B. Lahcen, O.H. Fahd, B. Amin, O. Aziz, Power forecasting of three silicon-based PV technologies using actual field measurements, Sustain. Energy Technol. Assess. 43 (2021), 100915, https://doi.org/10.1016/j.seta.2020.100915.
[55] Y. Yuan, C. Sun, M. Li, S.S. Choi, Q. Li, Determination of optimal supercapacitor-lead-acid battery energy storage capacity for smoothing wind power using empirical mode decomposition and neural network, Electr. Power Syst. Res. 127 (2015) 323–331, https://doi.org/10.1016/j.epsr.2015.06.015.